Macromolecules

ARTICLE

pubs.acs.org/Macromolecules

Macromolecular Diffusion in a Crowded Polymer Nanocomposite

Sangah Gam,[†] Jeffrey S. Meth,[‡] Steve G. Zane,[‡] Changzai Chi,[‡] Barbara A. Wood,[‡] Michelle E. Seitz,[†] Karen I. Winey,[†] Nigel Clarke,[§] and Russell J. Composto*[,†]

[†]Department of Materials Science and Engineering, University of Pennsylvania, Philadelphia, Pennsylvania 19104-6272, United States

[‡]DuPont Nanocomposite Technologies, Central Research & Development, E.I. DuPont de Nemours & Co., Inc., P.O. Box 400, Wilmington, Delaware, 19880-0400, United States

[§]Department of Physics and Astronomy, The University of Sheffield, Sheffield, S3 7RH, United Kingdom

Supporting Information

ABSTRACT: Macromolecular motion is reduced in crowded polymer nanocomposites. Tracer diffusion is measured for deuterated polystyrene (dPS) into a polystyrene (PS):silica nanoparticle (NP) matrix using elastic recoil detection. This nanocomposite is ideal for studying diffusion in a crowded system because the interparticle distance (ID) that defines confinement can be varied from much greater than to much less than the size of the dPS chain, which is described by $2R_g$, the radius of gyration, and varies from 10 to 40 nm in this study. Diffusion is observed to be significantly slower than that predicted by the Maxwell model. The tracer diffusion coefficient of dPS in the nanocomposite relative to the pure PS matrix (D/D_0) plotted against the NP separation relative to probe size (i.e., $ID/2R_g$) falls on a master curve, indicating that crowding is a property of both the dPS size and confinement in the nanocomposite. Moreover, the normalized diffusion coefficient decreases more rapidly when $ID/2R_g$ is less than ~1, suggesting strong confinement conditions. The scaling of the diffusion coefficient with chain length is in excellent agreement with the entropic barrier model that accounts for the slowing down associated with the loss of chain entropy due to constrictive bottlenecks.

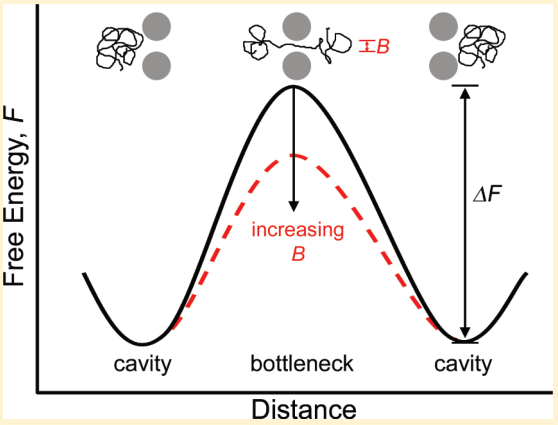

INTRODUCTION

Polymer nanocomposites, consisting of a polymer matrix reinforced with nanosized fillers, are used in numerous existing and emerging engineering applications to improve mechanical, thermal, and electrical properties.[1] As with traditional micro-sized fillers, effects of nanoparticles (NPs) on the mechanical properties depend primarily on the particle size, shape, polymer–filler interaction, and degree of dispersion in a polymer matrix. However, the inherently high surface-to-volume ratios associated with NPs can provide dramatically improved properties in polymer nanocomposites.[1−8] The enormous total interfacial area between NPs and polymer dictates that the interphase between polymer and NP becomes one of the dominant factors that determine the properties.[1,2,9,10] Another consequence of the high surface-to-volume ratio in polymer nanocomposites is the potential of NPs to alter polymer dynamics. In this study, we probe the effect of NPs on macromolecular diffusion as a function of interparticle distance and observe a slowing down that is stronger than that predicted by simple tortuosity.

Typically, molecular transport in heterogeneous media has been explained by applying the Maxwell model[11] for conductivity to describe diffusion. In this framework, the diffusion coefficient in composites with a sparse distribution of discrete particles decreases monotonically with filler concentration. However, the Maxwell model and subsequent refinement[12] do not account for the impact of changes to chain conformation in the vicinity of obstacles as a consequence of either entropic confinement or enthalpic interactions. Macromolecular diffusion in confined spaces such as gels and nanopores has been successfully described by the entropic barrier model (EBM).[13−16] Using Monte Carlo simulations and scaling arguments, it was shown that molecular diffusion through random media is slowed by bottlenecks which reduce the number of chain conformations and consequently the entropy available to the diffusing species. The EBM captures the diffusion of linear polymers through porous glasses filled with solvent.[17,18] Moreover, the electrophoretic mobility of star and ring polymers is well-described by the EBM, which predicts topological independence at moderate confinement conditions.[19] The present study demonstrates that macromolecular diffusion through a polymer with well-defined, closely spaced obstacles is successfully described by the EBM.

Received: October 28, 2010
Revised: February 25, 2011
Published: April 06, 2011

Macromolecular diffusion in confined media is also relevant for understanding the structure and function of biological[20−23] and bio-related[24−27] systems. For example, although the cytoplasm of cells contains proteins and RNA molecules that comprise 20−30% of the total volume,[21] molecules are still able to fold, assemble, and diffuse through such packed regions.[22] Protein transport across a cellular membrane,[23] m-RNA penetration into the nuclear membrane, and DNA injected from a virus into a cell all require translocation though constricted regions. In addition to *in vivo* biological processes, bio-related systems also utilize molecular diffusion in confined media. For example, diffusion of nucleic acid polymers through nanopores enables single-molecule detection.[24] DNA molecules can be separated using a microfabricated channel with many entropic traps that determines the translocation time.[25] Similarly, silicon membranes with nanopores impose size-based molecular separation of proteins,[26] and gel electrophoresis has long been used to separate DNA fragments.[27] Thus, understanding macromolecular diffusion in confined regions is of great interest for both biological and biorelated systems.

Although polymer dynamics in confining environments containing a polymer matrix have received some attention, a unified picture has yet to emerge, even within a given system. Using neutron scattering, Richter et al.[28,29] observed a slowing down of poly(ethylene oxide) intermediate time-scale chain dynamics confined within cylindrical pores for chain dimensions larger and smaller than the pore size. Using molecular dynamics simulations, Kumar et al.[30] found that polymer diffusion slowed down in the presence of NPs that attract the polymer, whereas diffusion was enhanced if this interaction was repulsive. Hu et al.[31] showed that the tracer diffusion of deuterated polystyrene (dPS) measured by secondary ion mass spectrometry was not affected by adding 5 vol % clay to a polystyrene (PS) matrix; however, the same amount of clay added to poly(methyl methacrylate) (PMMA) was found to reduce the diffusion coefficient by a factor of 3. For the tracer diffusion of dPS in a PS matrix containing carbon nanotubes (PS: CNT), Mu et al.[32,33] found that diffusion initially decreased, reached a minimum, and then recovered as CNT loading increased. The minimum diffusion coefficient was observed at a concentration corresponding to the percolation threshold. Segalman et al.[34] showed that tracer diffusion of dPS through a semicrystalline PS matrix scaled inversely with probe size, a result attributed to the entropic barriers imposed by crystalline domains. Green et al.[35] found that the diffusion of dPS or dPMMA into PS-*b*-PMMA is slower than that into homopolymer and attributed this behavior to the spatial orientation of the domains, volume fraction of matrix accessible to the homopolymer, and tortuosity of the domains.

Here, we study macromolecular diffusion through a crowded system consisting of well-dispersed silica NPs in a PS matrix. The crowding imposed by the NPs is controlled by varying the volume fraction of NP, ϕ_{NP}, from 0 to 0.5. A unique characteristic of this system is that a uniform dispersion is maintained even at 50 vol %. Thus, these nanocomposites are ideal for studying diffusion in a crowded system because the interparticle distance (ID) that defines confinement can be varied from much greater than to much less than the size of the macromolecular probe, $2R_g \sim 10$ to ~ 40 nm, where R_g is the radius of gyration. A significant result, enabled by our ability to vary the relative length scales over a wide range, is that the tracer diffusion coefficients in the nanocomposite relative to pure PS (D/D_0) plotted against the NP separation relative to probe size (i.e., $ID/2R_g$) falls on a master curve, indicating that crowding is a property of both the penetrant and the matrix. Moreover, the normalized diffusion coefficient decreases more rapidly when $ID/2R_g$ is less than ~ 1, suggesting strong confinement conditions. The scaling of the diffusion coefficient with chain length is in excellent agreement with the EBM,[13−15] which has not previously been applied to polymer melts with well-defined and tunable barriers.

EXPERIMENTAL METHODS

Preparation and Characterization of Polymer Nanocomposites. Polystyrene (M_w = 265 000 g mol^{-1}, polydispersity, PDI = 2.45) (PS) with phenyl-capped silica nanoparticles (NPs) is used as a matrix. These NPs were prepared using phenyltrimethoxysilane (PhTMS) as a coupling agent. The particle diameter and polydispersity were measured by dynamic light scattering (lognormal median = 28.7 nm, σ = 0.147), small angle x-ray scattering (lognormal median = 28.6 nm, σ = 0.115), and TEM (Gaussian median = 26.3 nm, σ = 0.159, N = 349). We denote the diameter as 28 nm in this paper. After synthesis, the PhTMS-capped silica particles were characterized using size exclusion chromatography (SEC) coupled with an IR absorption detector. The coverage of PhTMS was found to be 1.5 molecules nm^{-2}. Using densities of 1.099 g cm^{-3} for PS and 2.113 g cm^{-3} for NPs, the volume fractions of NP (ϕ_{NP}) in PS are 0, 0.01, 0.02, 0.05, 0.1, 0.2, 0.3, and 0.5. The PS and phenyl-capped silica NPs were each dissolved in dimethylacetamide (DMAC) or dimethylformamide (DMF) and then mixed at the appropriate ratio. Films were prepared by doctor blading the solution on a heated glass substrate ($\sim$100 °C) to form a film of thickness ~ 10 μm. The NP dispersion was observed using TEM after cross-sectioning the films using a microtome. Rutherford backscattering spectrometry (RBS) was used to obtain the depth profiles of the NPs in the composite film using 2 MeV He$^+$ at 10°. The depth resolution $\delta r = \delta E/[S_0]_{PNC}$ is 40−45 nm depending on silica NP loading, where S_0 is energy loss factor of the nanocomposite.[36] The NP concentration in the films was measured using thermogravimetric analysis (TGA). Thick films were prepared by hot pressing at $\sim$150 °C. For TGA measurements, films were heated at 20 °C min^{-1} to 400 °C and then held at 400 °C for 3 h.

The glass transition temperatures (T_g) of PS (265k) and the nanocomposites were measured using differential scanning calorimetry (DSC). Approximately $\sim$5 mg of material was placed in an aluminum pan. The scanning temperature range was 20−160 °C with a temperature ramp of 10 °C min^{-1} in a N_2 atmosphere. The T_g of pure PS (265k) was 105.2 ± 1 °C. For the nanocomposites, the T_g was 106.7 ± 0.4 °C, consistent with the findings of Bansal et al.[37] for PS:PS grafted silica NP nanocomposites. These studies show that the T_g of PS did not change appreciably with the addition of particles, and therefore, changes in diffusion coefficient are not due to changes in T_g.

Tracer Diffusion Couple and Processing. The tracer diffusion couples consisted of the nanocomposite matrix film covered with the thin dPS tracer film. The matrix film was removed from the glass substrate by floating in water and then picked up by a silicon substrate. The matrix film on silicon was preannealed at $\sim$150 °C for 3 days to age the film and remove any residual solvent. The dPS with molecular weights of 49 000 g mol^{-1} (PDI = 1.03), 168 000 g mol^{-1} (PDI = 1.03), and 532 000 g mol^{-1} (PDI = 1.05) was spin-coated on silicon substrates to produce $\sim$20 nm thick films as measured by ellipsometry. The dPS film was floated off in water and transferred onto the matrix film attached to the silicon substrate. Because of their wide range of diffusivities, the diffusion couples for dPS (49k), dPS (168k), and dPS (532k) were annealed in a vacuum oven at 145, 165, and 170 °C, respectively.

Molecular weight and polydispersity of PS and dPS were measured using SEC. The polymer was dissolved in tetrahydrofuran at various concentrations depending on its molecular weight.

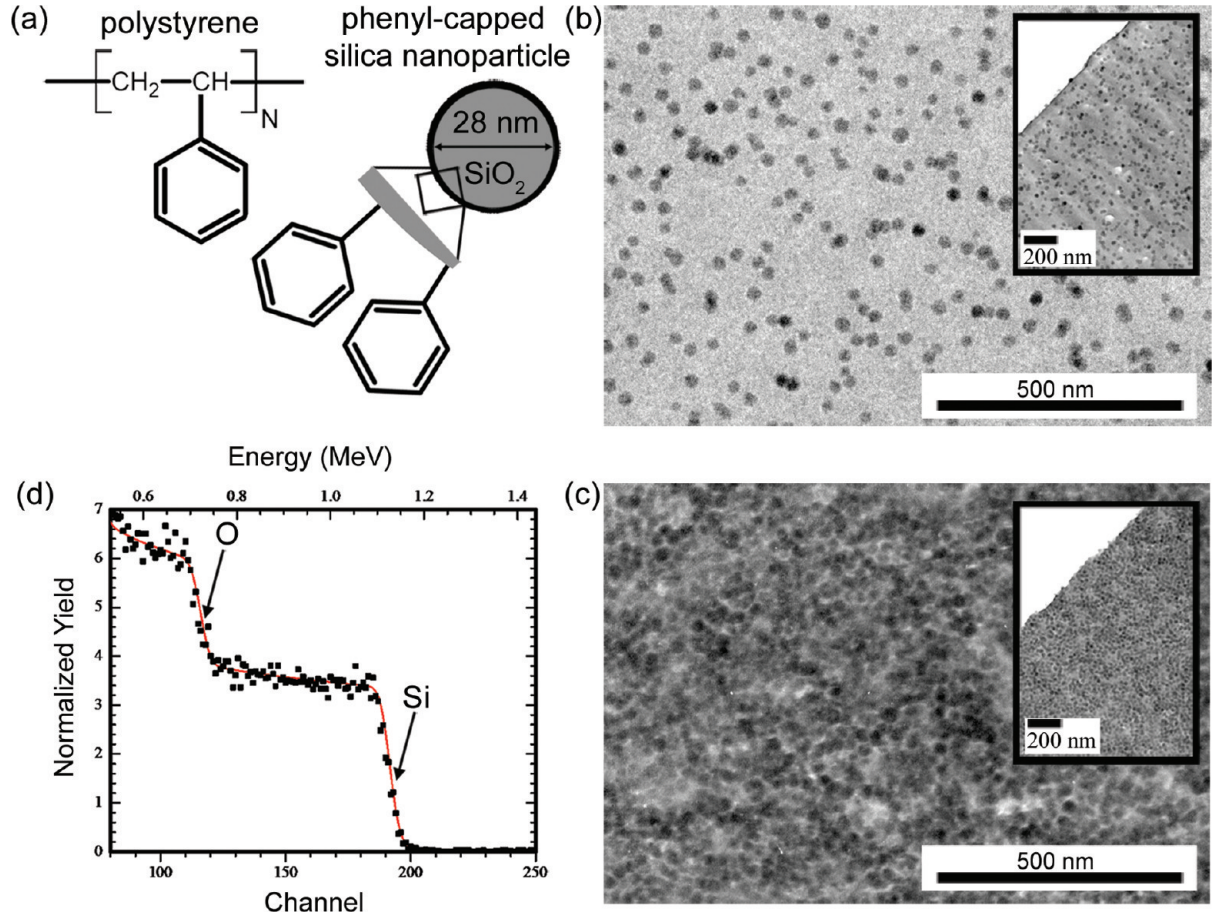

Figure 1. Characterization of PS:silica NP nanocomposites. (a) The chemical structure of PS (left) and a cartoon of the phenyl-capped silica NP (right). (b, c) Cross-sectional TEM images showing NP distribution for PS: $\phi_{NP} = 0.02$ and PS: $\phi_{NP} = 0.5$ nanocomposite films, respectively. Insets: cross-sectional TEM images of the near surface. Particles are uniformly dispersed in all nanocomposite films. (d) Silicon and oxygen concentration profile measured via RBS for PS ($\phi_{NP} = 0.5$) nanocomposite film. Closed square symbols represent the silicon and oxygen yield from the surface (arrows) and near surface (<2 μm) regions. The solid line is a simulation assuming a uniform distribution of NPs corresponding to a PS: $\phi_{NP} = 0.5$ nanocomposite film.

Elastic Recoil Detection (ERD). The dPS concentration profile in the matrix was measured by elastic recoil detection (ERD) and tracer diffusion coefficients obtained by fitting the profile to a one-dimensional (1-D) solution to Fick's second law equation for a finite source in a semi-infinite medium.[12,38] Diffusion coefficients were obtained from multiple measurements taken for each sample including those annealed at different times, and only the profiles having a sufficient diffusion length were considered. In ERD, the He^{2+} ion beam was accelerated to 3 MeV, and a 10 μm Mylar film was placed in front of the ERD detector to prevent the signal from the forward scattered He from masking the H and D signal. The incident beam intersects the plane of the sample at 15° and the recoiled H and D are collected by a solid-state detector. The ERD spectra of counts versus channel are converted to a dPS volume fraction profile using in-house software. The instrumental resolution is captured by the Gaussian function, $y = [1/\sigma(2\pi)^{1/2}] \exp(-x^2/2\sigma^2)$, where $\sigma = 39$ nm. The depth resolution and accessible depth are 78 nm and ~800 nm, respectively. In the least-squares fitting to determine D, χ^2 ranges from $\sim 10^{-3}$ to $\sim 10^{-4}$. Details of ERD have been reviewed elsewhere.[39]

RESULTS

Distribution of Nanoparticles in Polymer Nanocomposites. The fabrication of polymer nanocomposites with well-dispersed nanoparticles (NPs) is particularly challenging at high loadings. In our polymer nanocomposites, good dispersion is achieved by modifying the surface of silica NPs with phenyl groups that are similar to the pendant phenyl group found on the PS molecules in the matrix. Figure 1a shows the chemical structure of PS and a schematic of the phenyl-capped silica NPs, which have a diameter of 28 nm. The cross-sectional TEM image in Figure 1b shows that NPs are well dispersed at low concentration, $\phi_{NP} = 0.02$. Figure 1c shows that these NPs remain well dispersed even up to extremely high loading, $\phi_{NP} = 0.5$. We have also performed selected TEM studies on PNC's that were annealed for conditions corresponding to the diffusion experiments and observe no change in NP dispersion. As described later, the interparticle spacing for this crowded system is about 2 nm, which is a factor of ~0.2 and 0.05 smaller than the smallest and largest tracer molecules, respectively. The insets show that the sample surfaces have a similar distribution as the bulk.

To complement the lateral structure observed by TEM, depth profiles of the NPs were determined by RBS. Figure 1d shows the RBS spectra from a nanocomposite with $\phi_{NP} = 0.5$. The energy (channel) and normalized yield correspond to depth and elemental concentration, respectively. The silicon and oxygen atoms located at the surface of the film are denoted with arrows. For both elements, the normalized yield is consistent with a uniform distribution of NPs. Using XRUMP, the spectrum was

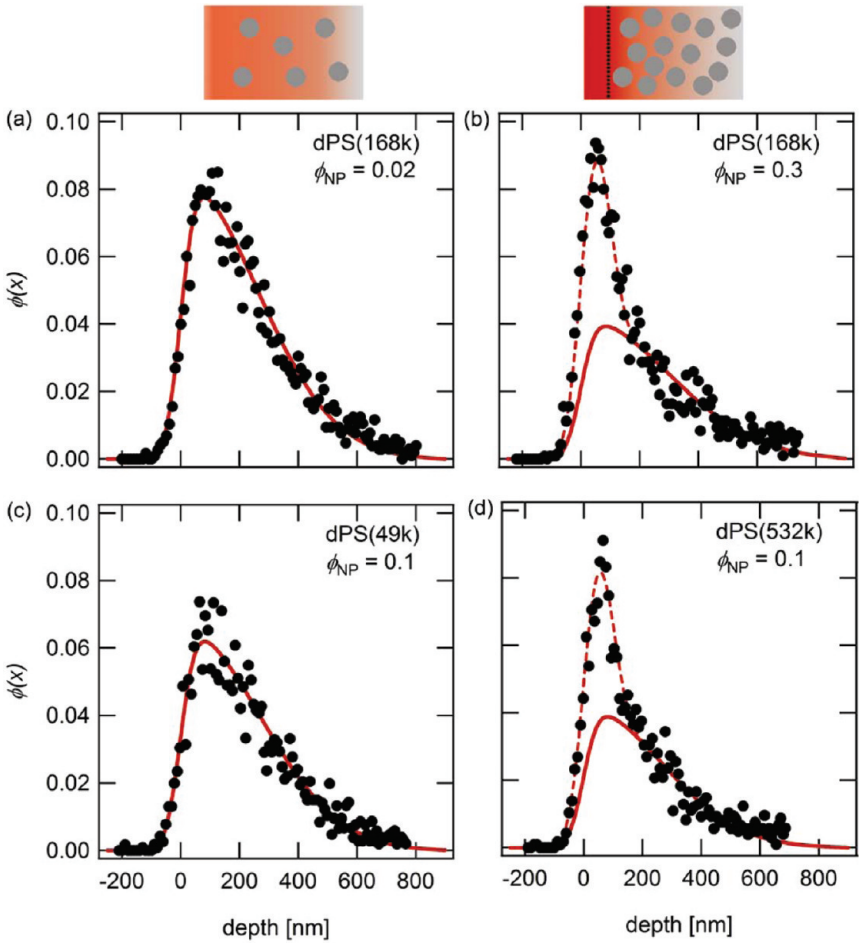

Figure 2. Diffusion profiles of dPS in PS:NP nanocomposites measured using ERD to investigate the effect of NP volume fraction and tracer molecular weight. Solid line is a fit of experimental data with eq 1 using appropriate D values, whereas the dashed line represents the sum of the solid line and a surface peak. Tracer molecular weight (M) and NP volume fraction (ϕ_{NP}) are denoted in the legends. (a) $D = 2.3 \times 10^{-14}$ cm^2 s^{-1} at 165 °C. (b) $D = 9.8 \times 10^{-15}$ cm^2 s^{-1} at 165 °C. (c) $D = 1.4 \times 10^{-14}$ cm^2 s^{-1} at 145 °C. (d) $D = 3.8 \times 10^{-15}$ cm^2 s^{-1} at 170 °C. Note that surface peaks are observed for profiles in Figure 2b,d. The cartoons (top) represent the tracer and matrix conditions that correspond to diffusion profiles without (left) and (right) with a surface peak.

simulated (solid line) using a nanocomposite film (>2 μm) containing 50 vol % of NPs uniformly dispersed in 50 vol % PS.[40] The depth resolution is 38 nm.[36] The simulation is in excellent agreement with the RBS data and shows that NPs are uniformly distributed in the near-surface region (i.e., no depletion or enrichment), consistent with TEM observations. We have also performed RBS on selected PNC's that were annealed for conditions corresponding to the diffusion experiments and observe no change in NP dispersion within the resolution of RBS. These TEM and RBS results are representative of nanocomposite films at all NP loadings, demonstrating that phenyl-capped silica NPs are uniformly distributed at length scales probed by the diffusion studies, as required to quantitatively interpret the diffusion results. Furthermore, using the Stokes−Einstein equation and the appropriate PS viscosity,[41,42] the NP diffusion coefficient at 170 °C is 4.0×10^{-17} cm^2 s^{-1}. This is much smaller than the dPS diffusion coefficient at 170 °C, which ranges from 10^{-12} to 10^{-15} cm^2 s^{-1}. Thus, the NPs are nearly immobile relative to the tracer molecules which diffuse ~300 nm. Using TEM and RBS, we have established that these PS-based nanocomposites are model materials with well-dispersed NPs that persist throughout the diffusion experiments.

Tracer Diffusion in Nanocomposites. Macromolecular diffusion through the nanocomposites was investigated using tracer diffusion experiments. A thin dPS layer (~20 nm) was deposited on a thick (~10 μm) nanocomposite film. The dPS volume fraction profiles, $\phi(x)$, were determined using ERD after annealing, as we have described recently.[32,33] The tracer diffusion coefficient (D) was determined by fitting the experimental $\phi(x)$ with the appropriate solution to Fick's second law. For an initial tracer thickness h, $\phi(x)$ is given by[12,38]

$$\phi(x) = \frac{1}{2}\left[\mathrm{erf}\left(\frac{h-x}{\sqrt{4Dt}}\right) + \mathrm{erf}\left(\frac{h+x}{\sqrt{4Dt}}\right)\right] \qquad (1)$$

where erf denotes the error function and t is annealing time. This expression was convoluted with a Gaussian function whose standard deviation corresponds to the depth resolution of 78 nm. Using least-squares fitting, D is varied until the simulation matches the experimental profile by minimizing χ^2.

The effect of confinement on diffusion can be evaluated by determining how the tracer diffusion coefficient depends on both the volume fraction of NP (ϕ_{NP}) in the nanocomposite matrix and the molecular weight of the tracer (M). To test the former,

dx.doi.org/10.1021/ma102463q |*Macromolecules* 2011, 44, 3494–3501

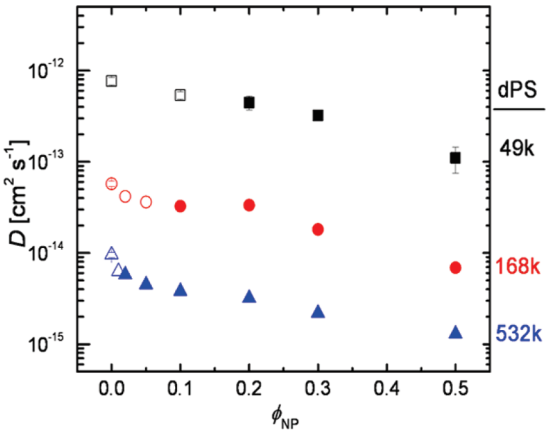

Figure 3. Diffusion coefficient versus NP loading. Diffusion coefficients of dPS (M = 49k, 168k, and 532k) at 170 °C are plotted as a function of NP volume fraction. Closed and open symbols represent diffusion with and without surface peaks, respectively. The error bars represent the standard deviation determined from measurements taken on samples annealed for different times.

dPS (M = 168k) was diffused into nanocomposite films containing ϕ_{NP} = 0.02 and 0.3 by annealing at 165 °C for 4 and 12.5 h, respectively. Whereas the dPS profile shown in Figure 2a follows the expected Fickian diffusion shape at ϕ_{NP} = 0.02, the dPS profile for diffusion into the matrix at the higher loading exhibits a surface peak as shown in Figure 2b. The surface peak results from a reduced flux at the interface possibly caused by some additional crowding of the NPs. The reduced flux scales with the volume fraction of NPs, and therefore the surface peak becomes more pronounced as loading increases. Our observation that, as annealing time increases (i.e., dPS penetration into the matrix increases), the surface peak decreases (as shown in Supporting Information Figure S1) is also consistent with this mechanism. A more detailed theoretical and experimental investigation of the origins of the surface peak will be the subject of a future publication. Segalman et al.[34] also observed a surface peak for diffusion into semicrystalline polymers wherein the crystalline domains are effectively impenetrable. The solid lines in Figures 2a and 2b represent best fits of the experimental data with eq 1 with $D = 2.3 \times 10^{-14}$ and 9.8×10^{-15} cm^2 s^{-1}, respectively. The dashed line in Figure 2b represents the sum of the solid line and a surface peak from a reduced flux due to the impenetrable NPs. Thus, at fixed tracer molecular weight, the diffusion coefficient is reduced by a factor of ~2 as ϕ_{NP} increases from 0.02 to 0.3, consistent with slowing down due to greater confinement.

To investigate the effect of tracer size, dPS with M = 49k and 532k was diffused into nanocomposites having a fixed NP concentration of ϕ_{NP} = 0.1. Figures 2c and 2d show the volume fraction profiles after annealing at 145 °C for 7 h and 170 °C for 25 h, respectively. The temperatures and times are selected to provide an optimum diffusion distance of ~300 nm for ERD measurements. In Figure 2c, the depth profile of the shorter tracer chains shows a Fickian type profile (solid line), whereas the profile for the longer chains (dashed line) in Figure 2d indicates a surface peak overlapping with the Fickian type profile (solid line). Thus, a surface peak is observed either when the matrix is crowded (i.e., high ϕ_{NP}) or at large probe sizes (i.e., high M), as noted in Figures 2b and 2d, respectively.

The dPS tracer diffusion coefficients are shown in Figure 3 for M = 49k, 168k, and 532k at 170 °C. Diffusion coefficients for dPS (49k) and dPS (168k) measured at 145 and 165 °C, respectively, were converted to values at 170 °C using the Vogel−Fulcher equation.[43] To test the role of matrix molecular weight polydispersity, tracer diffusion measurements in nanocomposites containing PS (M_w = 400 000 g mol^{-1}, PDI = 1.06) were performed. These studies are in agreement with the data shown in Figure 3, indicating that polydispersity does not significantly affect diffusion in PNCs containing entangled polymers. As M increases from 49k to 532k, Figure 3 shows that the diffusion coefficient decreases strongly at a fixed ϕ_{NP}. As ϕ_{NP} increases, the diffusion coefficient decreases for all dPS molecular weights. At low loadings, $\phi_{NP} < 0.1$, this reduction in D becomes stronger as M increases, consistent with greater slowing down of larger molecules as they squeeze past constraints. For example, D decreases by 30% and 60% as M increases from 49k to 532k at ϕ_{NP} = 0.1. The open symbols in Figure 3 denote diffusion couples with volume fraction profiles captured by Fickian diffusion (i.e., eq 1), whereas the closed symbols represent couples that exhibit a surface peak. As M increases, the maximum volume fraction of NP at which eq 1 fits the dPS profile decreases from 0.1 to 0.01 as M increases from 49k to 532k, respectively. In summary, larger molecules are more strongly influenced by diffusion in confined media than smaller ones.

The two length scales that are relevant for the diffusion of probe molecules through bottlenecks are[44,45] (1) the molecular size, which for polymers corresponds to the radius of gyration, and (2) the bottleneck size, or in the case of a polymer nanocomposite, where confinement is imposed by the discrete, impenetrable particles (cf. Figure 2, top), the average interparticle distance, ID, between particles. Assuming that NPs are randomly distributed in the polymer matrix, ID is given by[46]

$$ID = d\left[\left(\frac{2}{\pi\phi_{NP}}\right)^{1/3} - 1\right] \qquad (2)$$

where d is the NP diameter (28 nm). As shown in Figure 4a, ID initially decreases strongly, by nearly an order of magnitude, as ϕ_{NP} increases from 0.01 to 0.20, and then decreases more slowly between 0.20 and 0.50. The symbols represent the NP volume fractions that satisfy the confinement condition $ID \sim 2R_g$. For M = 49k, 168k, and 532k, this condition is satisfied at ϕ_{NP} = 0.23, 0.12, and 0.05, respectively. The probe is considered to be diffusing in a crowded matrix if $ID < 2R_g$; e.g., the probe size is larger than the spacing between NPs. For example, diffusion of dPS (49k) is highly constrained for $\phi_{NP} > 0.23$ because molecules must undergo large conformational energy changes to squeeze between NPs spaced closer than $2R_g$. As M increases, the concentration of NP that induces strong confinement decreases. Thus, comparing diffusion in nanocomposites as a function of the reduced variable $ID/2R_g$ should be insightful.

Motivated by the confinement conditions described above, Figure 4b shows that all data collapse onto a master curve when the reduced diffusion coefficient (D/D_0), where D is normalized by the tracer diffusion coefficient in pure PS (D_0), is plotted against the dimensionless quantity $ID/2R_g$. As $ID/2R_g$ decreases from 3 to ~1.5, D/D_0 decreases weakly. This regime mainly represents diffusion couples that exhibit diffusion profiles without a surface peak (open symbols). For $ID/2R_g < 1$ (i.e., crowded conditions), D/D_0 decreases strongly as $ID/2R_g$ decreases. This regime corresponds to diffusion couples that exhibit a surface

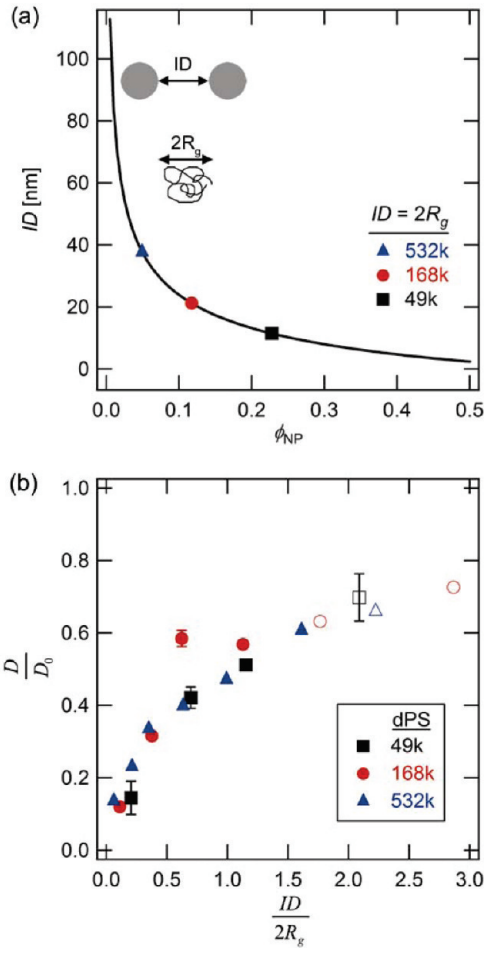

Figure 4. Effect of relative size of probe and interparticle distance on diffusion. (a) Interparticle distance (ID) is plotted as a function of the volume fraction of NP (ϕ_{NP}) under the assumption that NPs are randomly distributed in a polymer matrix according to eq 2. (b) Reduced diffusion coefficients (D/D_0) of dPS (M = 49k, 168k, and 532k) plotted against $ID/2R_g$ fall on a master curve. Closed and open symbols represent diffusion with and without surface peaks, respectively. The error bars represent the standard deviation determined from measurements taken on samples annealed for different times.

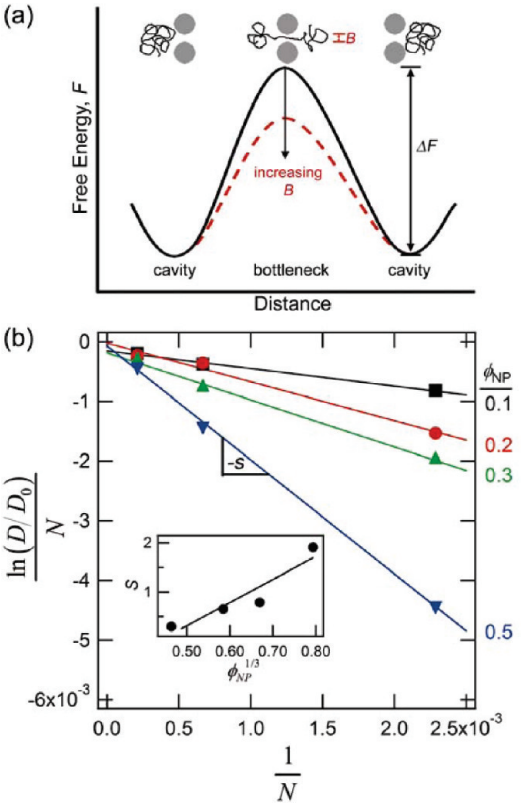

Figure 5. Entropic barrier model. (a) Free energies and chain conformations as a probe chain diffuses from one cavity to another cavity through a bottleneck of size B. In the bottlenecks, the number of chain conformations is reduced resulting in the formation of an energy barrier with a height ΔF that depends on the size of the bottleneck. (b) $\ln(D/D_0)/N$ is plotted against $1/N$ at ϕ_{NP} = 0.1, 0.2, 0.3, and 0.5, where N is the degree of polymerization of the tracer. Inset: slope s vs $\phi_{NP}^{1/3}$ ($\sim ID^{-1}$). This scaling behavior is in agreement with the entropic barrier model.

peak (closed symbols). This strong slowing down may be attributed to the loss of chain conformations as tracer molecules squeeze between closely spaced NPs.

Applying the Entropic Barrier Model. While the collapse of the data onto a master curve provides a valuable empirical representation of the dynamics of polymers in confined systems, we turn our attention to the entropic barrier model (EBM) to gain insight into the underlying physical mechanisms. Prior to this work, the EBM has not been applied to polymer melts with well-defined and tunable barriers because of the difficulty in fabricating uniformly distributed barriers at high loadings. In our nanocomposites, the spaces between NPs define cages or cavities that enclose dPS chains either in whole or in part, depending on the NP concentration and the corresponding cage size. In the framework of the EBM, the cavities are separated by bottlenecks (i.e., entropic barriers) as illustrated in Figure 5a, and macromolecular diffusion through random media such as porous glasses, concentrated polymer solutions, gels, and semicrystalline polymers deviates from reptation behavior because the media contains entropic traps that perturb chain dynamics. As noted earlier, the NPs are capped with phenyl groups, and therefore enthalpic interactions with tracer chains should be small. Thus, the free energy barrier ΔF in Figure 5a should be dominated by the loss of chain conformations as chains pass through bottlenecks formed by neighboring NPs. For an activated process $D = D_0 \exp(-\Delta F/k_B T)$, where D_0 represents diffusion without barriers (i.e., $\phi_{NP} = 0$). Because chain motion occurs between cavities of size C, separated by bottlenecks of size B, the diffusion coefficient decreases exponentially with ΔF ($= F_2 - F_1$), where F_1 and F_2 are the confinement free energy for a chain in a cavity and bottleneck, respectively. According to scaling arguments, F_1 and F_2 are proportional to $NC^{-1/\nu}$ and $NB^{-1/\nu}$, where N is the degree of polymerization and ν is 0.5 for a Gaussian chain.[42] The scaling form for D/D_0 is given by[13−15]

$$\ln(D/D_0)/N = A - s/N \qquad (3)$$

where s is proportional to $B^{-1}(1 - z^{-1}(B/C)^{1/\nu})$ and z is the average number of cavities containing unconfined segments per bottleneck. For $20 \leq N \leq 80$, Monte Carlo simulations[13−15] to determine D agree with the scaling predictions of eq 3 and exhibit a slope that increases as the bottleneck size, B, decreases.

To test if the EBM captures dPS diffusion in nanocomposite matrices, $\ln(D/D_0)/N$ is plotted against $1/N$ for ϕ_{NP} = 0.1, 0.2,

dx.doi.org/10.1021/ma102463q |Macromolecules 2011, 44, 3494–3501

0.3, and 0.5. Figure 5b shows that the EBM scaling relationship is in good agreement with the experimental data. For tracer diffusion into a semicrystalline polymer, Segalman[34] also observed that D decreases as $1/N$, consistent with the EBM. However, because the barrier dimensions were ill defined for that system, a rigorous test of the EBM model was not possible. Figure 5b also shows that the slope, s, increases as ϕ_{NP} increases in qualitative agreement with eq 3. Since $s \sim B^{-1}$ and B is determined by ID, we can relate s to ϕ_{NP} via eq 2, namely $s \sim B^{-1} \sim ID^{-1} \sim \phi_{NP}^{1/3}$. The inset of Figure 5b shows that s increases linearly with $\phi_{NP}^{1/3}$, indicating that an increase in NP loading does indeed slow down tracer diffusion in accordance with the EBM. Thus, our studies are a systematic experimental verification of the relationship between the slope, s, and the confining media.

In applying the EBM model, several assumptions are made. First, we use eq 2 to estimate an average ID that is used in the EBM model. A log normal distribution of ID values is likely and correspondingly a distribution of bottleneck and cavity sizes. Ultrasmall-angle X-ray scattering studies are in progress to quantify the spatial distribution of NPs as a function of loading. Second, enthalpic contributions could influence diffusion behavior. For example, polymer diffusion along an attractive surface is slower than through the bulk.[47] Also, molecular dynamics simulations show that chain diffusion can be enhanced or reduced when interactions are repulsive or attractive, respectively.[30] Because NPs in this study are capped with phenyl groups to minimize interactions with dPS, the interaction between NP and tracer molecule should be weak. Third, Muthukumar[48] modified the original EBM to include enthalpic interactions and found that for a polymer escaping from a nanopore the entropic barrier mechanism dominates for short pores while pore−polymer interactions dominant for pores longer than a critical length. The narrowest section of the bottleneck as noted in Figure 5a is relatively short, further justifying the use of the EBM for describing dPS diffusion in crowded nanocomposites. While both the master curve and EBM capture experimental results, a quantitative relationship between these two descriptions of polymer diffusion in crowded systems is of great interest and the subject of future study.

CONCLUSIONS

Polymer diffusion was investigated in nanocomposites containing silica nanoparticles (NPs). The lateral and depth distributions of the NPs were found to be uniform, even at 50 vol % NP, indicating that nanocomposites are a model system for testing how macromolecules diffuse through crowded systems. Tracer diffusion slows down as NP loading increases, and this reduction is strongest for the largest tracer chains. Significantly, we find that the reduced diffusion coefficient, D/D_0, collapses onto a master curve when plotted versus $ID/2R_g$, indicating that confinement is determined by the spacing between particles relative to the size of the tracer molecule. Our results are in excellent agreement with the entropic barrier model, indicating that the slowing down of the molecular diffusion in the presence of NPs is mainly attributed to the loss of chain conformations as molecules squeeze through bottlenecks formed by neighboring particles. These studies of diffusion in a crowded system inspire a series of future studies including the effect of particle shape on tracer diffusion[32,33,49] as well as designing polymer nanocomposites having interactions between the tracer molecules and particles. Such studies are technologically important for ultrafiltration, DNA separation, and melt processing of polymer nanocomposites and also can provide new insight into the dynamics of biological systems where macromolecular crowding is ubiquitous.

ASSOCIATED CONTENT

Supporting Information. Figure S1. This material is available free of charge via the Internet at http://pubs.acs.org.

AUTHOR INFORMATION

Corresponding Author
*E-mail: composto@seas.upenn.edu.

ACKNOWLEDGMENT

This research was funded primarily by the National Science Foundation NSF/EPSRC Materials World Network DMR-0908449. Support was also provided by the NSF/MRSEC-DMR05-20020 (K.I.W., R.J.C.) and Polymer Programs DMR05-49307 (R.J.C.) as well as the EP/G065373/1 (N.C.). We thank Prof. Bradford B. Wayland (University of Pennsylvania, Temple University) for use of size exclusion chromatography. We thank Professors Timothy Lodge, Edward Kramer, Murugappan Muthukumar, Peter Green, and Charles Han for useful comments.

REFERENCES

(1) Winey, K. I.; Vaia, R. A. *MRS Bull.* **2007**, *32* (4), 314–319.
(2) Vollenberg, P. H. T.; Heikens, D. *Polymer* **1989**, *30* (9), 1656–1662.
(3) Chan, C. M.; Wu, J. S.; Li, J. X.; Cheung, Y. K. *Polymer* **2002**, *43* (10), 2981–2992.
(4) Gersappe, D. *Phys. Rev. Lett.* **2002**, *89* (5), 058301.
(5) Su, S. P.; Jiang, D. D.; Wilkie, C. A. *Polym. Adv. Technol.* **2004**, *15* (5), 225–231.
(6) Reynaud, E.; Jouen, T.; Gauthier, C.; Vigier, G.; Varlet, J. *Polymer* **2001**, *42* (21), 8759–8768.
(7) Park, J. H.; Jana, S. C. *Polymer* **2003**, *44* (7), 2091–2100.
(8) Stojanovic, D.; Orlovic, A.; Markovic, S.; Radmilovic, V.; Uskokovic, P. S.; Aleksic, R. *J. Mater. Sci.* **2009**, *44* (23), 6223–6232.
(9) Ciprari, D.; Jacob, K.; Tannenbaum, R. *Macromolecules* **2006**, *39*, 6565–6573.
(10) Schadler, L. S.; Kumar, S. K.; Benicewicz, B. C.; Lewis, S. L.; Harton, S. E. *MRS Bull.* **2007**, *32* (4), 335–340.
(11) Maxwell, J. C.; Thomson, J. J. *A Treatise on Electricity and Magnetism*; Unabridged 3rd ed.; Dover Publications: New York, 1954; p 2 v. in 1.
(12) Crank, J. *The Mathematics of Diffusion*, 2nd ed.; Clarendon Press: Oxford, 1975; p viii, 414 pp.
(13) Muthukumar, M.; Baumgartner, A. *Macromolecules* **1989**, *22* (4), 1937–1941.
(14) Muthukumar, M.; Baumgartner, A. *Macromolecules* **1989**, *22* (4), 1941–1946.
(15) Muthukumar, M. *J. Non-Cryst. Solids* **1991**, *131*, 654–666.
(16) Muthukumar, M. *Phys. Rev. Lett.* **2001**, *86* (14), 3188–3191.
(17) Easwar, N. *Macromolecules* **1989**, *22* (8), 3492–3494.
(18) Guo, Y. H.; Langley, K. H.; Karasz, F. E. *Macromolecules* **1990**, *23* (7), 2022–2027.
(19) Hoagland, D. A.; Muthukumar, M. *Macromolecules* **1992**, *25* (24), 6696–6698.
(20) Alberts, B. *Molecular Biology of the Cell*; Garland Pub.: New York, 1983; p xxxix, 1146, 35 pp.
(21) Bernado, P.; de la Torre, J. G.; Pons, M. *J. Mol. Recognit.* **2004**, *17* (5), 397–407.

(22) Rivas, G.; Ferrone, F.; Herzfeld, J. *EMBO Rep.* **2004**, *5* (1), 23–27.
(23) Schatz, G.; Dobberstein, B. *Science* **1996**, *271* (5255), 1519–1526.
(24) Branton, D.; Deamer, D. W.; Marziali, A.; Bayley, H.; Benner, S. A.; Butler, T.; Di Ventra, M.; Garaj, S.; Hibbs, A.; Huang, X. H.; Jovanovich, S. B.; Krstic, P. S.; Lindsay, S.; Ling, X. S. S.; Mastrangelo, C. H.; Meller, A.; Oliver, J. S.; Pershin, Y. V.; Ramsey, J. M.; Riehn, R.; Soni, G. V.; Tabard-Cossa, V.; Wanunu, M.; Wiggin, M.; Schloss, J. A. *Nature Biotechnol.* **2008**, *26* (10), 1146–1153.
(25) Han, J.; Craighead, H. G. *Science* **2000**, *288* (5468), 1026–1029.
(26) Striemer, C. C.; Gaborski, T. R.; McGrath, J. L.; Fauchet, P. M. *Nature* **2007**, *445* (7129), 749–753.
(27) Southern, E. M. *J. Mol. Biol.* **1975**, *98* (3), 503–517.
(28) Krutyeva, M.; Martin, J.; Arbe, A.; Colmenero, J.; Mijangos, C.; Schneider, G. J.; Unruh, T.; Su, Y.; Richter, D. *J. Chem. Phys.* **2009**, *131* (17), 174901.
(29) Martin, J.; Krutyeva, M.; Monkenbusch, M.; Arbe, A.; Allgaier, J.; Radulescu, A.; Falus, P.; Maiz, J.; Mijangos, C.; Colmenero, J.; Richter, D. *Phys. Rev. Lett.* **2010**, *104* (19), 197801.
(30) Desai, T.; Keblinski, P.; Kumar, S. K. *J. Chem. Phys.* **2005**, *122* (13), 134910.
(31) Hu, X. S.; Zhang, W. H.; Si, M. Y.; Gelfer, M.; Hsiao, B.; Rafailovich, M.; Sokolov, J.; Zaitsev, V.; Schwarz, S. *Macromolecules* **2003**, *36* (3), 823–829.
(32) Mu, M. F.; Clarke, N.; Composto, R. J.; Winey, K. I. *Macromolecules* **2009**, *42* (18), 7091–7097.
(33) Mu, M. F.; Composto, R. J.; Clarke, N.; Winey, K. I. *Macromolecules* **2009**, *42* (21), 8365–8369.
(34) Segalman, R. A.; Jacobson, A.; Kramer, E. J.; Lustig, S. R. *Macromolecules* **2004**, *37*, 2613–2617.
(35) Green, P. F.; Russell, T. P.; Jerome, R.; Granville, M. *Macromolecules* **1988**, *21* (11), 3266–3273.
(36) Chu, W.-K.; Mayer, W.; Nicolet, M.-A. *Backscattering Spectrometry*; Academic Press: New York, 1978; p xv, 384 pp.
(37) Bansal, A.; Yang, H.; Li, C.; Cho, K.; Benicewicz, B. C.; Kumar, S. K.; Schadler, L. S. *Nature Mater.* **2005**, *4* (9), 693–698.
(38) Green, P. F.; Mills, P. J.; Kramer, E. J. *Polymer* **1986**, *27* (7), 1063–1066.
(39) Composto, R. J.; Walters, R. M.; Genzer, J. *Mater. Sci. Eng. R* **2002**, *38* (3−4), 107–180.
(40) Doolittle, L. R. *Nucl. Instrum. Methods B* **1985**, *9* (3), 344–351.
(41) Miller, A. A. *J. Polym. Sci., Part A-2: Polym. Phys.* **1968**, *6* (6), 1161–1175.
(42) Rubinstein, M.; Colby, R. H. *Polymer Physics*; Oxford University Press: New York, 2003; p xi, 440 pp.
(43) Green, P. F.; Kramer, E. J. *J. Mater. Res.* **1986**, *1* (1), 202–204.
(44) Ogston, A. G.; Preston, B. N.; Wells, J. D.; Snowden, J. M. *Proc. R. Soc. London, A* **1973**, *333* (1594), 297–316.
(45) Sartori, A.; Barbier, V.; Viovy, J. L. *Electrophoresis* **2003**, *24* (3), 421–440.
(46) Wu, S. H. *Polymer* **1985**, *26* (12), 1855–1863.
(47) Zheng, X.; Rafailovich, M. H.; Sokolov, J.; Strzhemechny, Y.; Schwarz, S. A.; Sauer, B. B.; Rubinstein, M. *Phys. Rev. Lett.* **1997**, *79* (2), 241–244.
(48) Muthukumar, M. *J. Chem. Phys.* **2003**, *118* (11), 5174–5184.
(49) Pryamitsyn, V.; Ganesan, V. *Phys. Rev. Lett.* **2008**, *100* (12), 128302.